Experimental and analytical study of bond between basalt FRP bars and geopolymer concrete

Giulia Trabacchin, Wendel Sebastian, Mingzhong Zhang*

Department of Civil, Environmental and Geomatic Engineering, University College London, London WC1E 6BT, UK

Abstract: This paper presents an experimental and analytical study of the bond behaviour of basalt fibre reinforced polymer (BFRP) bars in geopolymer concrete (GPC). Pull-out tests were conducted on ribbed BFRP bars embedded in GPC cubes considering different bar diameters (6, 8 and 10 mm) and embedment lengths ($5d_b$, $10d_b$ and $15d_b$) to investigate their effects on bond behaviour in terms of bond-slip response, bond strength and failure mechanisms. Results indicate that the chemical adhesion is low, and the bond is mainly dependent on mechanical interlocking which stopped when pullout occurred by local crushing of the GPC with the BFRP ribs remaining undamaged, suggesting high rib shear strength. A theoretical bilinear model was used to describe the local bond-slip relationship and the bond interface properties. There exists nonlinear bond stress distribution, especially for longer embedment lengths and lower load levels with a bond stress concentration factor of 3.9. A parametric study was performed to estimate the influences of bar diameter, embedment length and elastic modulus on maximum pull-out load, based on which the load transfer mechanisms between BFRP bars and GPC were explored, and a formula for predicting the bond strength was proposed in comparison with experimental data.

Keywords: Fibre reinforced polymer; Alkali-activated concrete; Bond strength; Analytical analysis; Theoretical prediction

1. Introduction

Steel reinforced Portland cement concrete (PCC) is the most widely used construction material in the world. As the binding material in concrete, Portland cement is responsible for around 7% of global CO_2 emissions [1]. To improve the sustainability of concrete, different alternative binding materials to Portland cement have been proposed. Among them, geopolymer, also known as alkali-activated materials, made from industrial by-products such as fly ash (FA) and ground granulated blast-furnace slag (GGBS) is considered as a promising alternative [2], the use of which as a substitute for Portland cement for concrete can help reduce CO_2 emissions by up to 80% compared to PCC [3]. Another issue with reinforced concrete is inadequate durability due to corrosion of steel reinforcement, which has an estimated global cost of $2.5 trillion [4,5]. In recent years, basalt fibre reinforced polymer (BFRP) bars have been introduced as an alternative reinforcement to steel bars because of their light weight, high tensile strength, excellent resistance to acids and corrosion, and a wide range of working temperatures [6]. Considering the promising properties, the combination of GPC and BFRP bars has

* Corresponding author. E-mail address: mingzhong.zhang@ucl.ac.uk (M. Zhang)

been recently proposed as a sustainable and durable building system for the construction industry [7–9].

The bond between reinforcement and concrete is a key property that strongly influences the structural performance of reinforced concrete structures. The load transfer between reinforcement and concrete is generally characterised by the local bond-slip curve, which can be determined using either pull-out or beam-end tests [10]. To date, many studies have been conducted to investigate the bond-slip behaviour of steel reinforced GPC and BFRP reinforced PCC systems using pull-out and beam-end tests, while the bond between BFRP bars and GPC has not been explored. The bond slip curves for steel reinforcement in GPC and PCC are similar in shape, but with up to 40% more bond strength in GPC, which can be attributed to the more homogenous and dense microstructure of GPC [11–14]. Thus, GPC is not only more sustainable than PCC but may also offer superior structural performance.

The bond-slip behaviour of fibre reinforced polymer (FRP) in PCC is more complex than steel rebars, owing to the potential influences of fibre type, resin type, anisotropic feature and surface treatment of FRP [6,15,16]. Previous pull-out tests on BFRP reinforced PCC indicated that BFRP bars developed an average bond strength of 75% of glass FRP (GFRP) bars but higher residual stress [17]. Increasing bar diameter and embedment length increased the maximum pull-out load but reduced the average bond strength [18,19]. The reduction in bond stress can be ascribed to the higher interface surface area, non-uniform distribution of the shear bond stress along the bar embedded portion and shear lag effect [20,21]. Excellent bond durability of BFRP bars in PCC was proven where after 45 days of exposure to alkaline environment, vinyl-ester-made BFRP bars and GFRP bars experienced similar a bond strength retention (92.4 %), while the bond stress retention of epoxy-made BFRP bars was relatively higher (139.5%) [22]. Several other studies [22–25] also demonstrated that BFRP bars have comparable or higher bond durability than the similar GFRP bars. The superior bond properties of BFRP bars support their application as internal reinforcement in concrete, although they have not been included in the design codes available for other FRP reinforcements [26–29].

As the use of strain gauges or distributed optical fibre sensors [26–30] has been proven to have limited efficacy for the experimental assessment of bond stress distribution [31], the analytical study appears to be a more helpful tool. The most well-known bond-slip constitutive models for the FRP reinforced concrete include the Malvar model [32], the modified BPE model [20,33] and the CMR model [34], calibrated from pull-out tests with short embedment lengths of bar in concrete. It is worth pointing out that the set of values defining the bond-slip constitutive law are identified based on non-local measurements such as the average bond stress that does not account for the shear stress nonlinear distribution along the bar embedded portion. It is still a debate whether the parameters defining the bond-slip law should be derived from samples with shorter ($5d_b$) or longer ($>5d_b$) embedment length. To avoid the influences of significant deformation and damage of concrete on the local bond-slip

curve and to obtain a relatively uniform bond stress distribution, it is recommended to derive the bond-slip law from samples with short embedded length ($5d_b$) [35–37]. On the contrary, for shorter embedment length, the local imperfections at the interface could have a strong influence on the bond-slip curve, resulting in scattered values of τ_m and s_m. Therefore, to minimise the effect of local imperfections, the use of longer embedment lengths was suggested to calibrate the bond-slip constitutive law [38].

The analytical solutions to governing differential equations for different systems need to be derived to compute the interface properties. Focacci et al. [39] provided the analytical solution to calculate the slip and bond stress profiles along the bar based on the mBPE and CMR bond-slip laws. A closed-form solution can be determined if the embedment length is longer than the development length, i.e. if the slip at the free end of the bar is zero. When some slip is recorded at the bar free end, the differential equation must be solved numerically [38,39]. A multilinear model was proposed for GFRP bars in high-performance steel fibre reinforced self-compacting concrete [35], which accounts for the high stiffness induced by the chemical adhesion in the initial stage of the bond-slip curve and the friction phase after the softening. The stress distribution of GFRP bars in concrete was predicted using a linear model [40], which can only provide the constitutive behaviour at the serviceability state level as it lacks a definition for the descending branch. To the best of the authors' knowledge, the bond behaviour of BFRP bars in GPC has not yet been investigated analytically.

The main purpose of this study is to investigate experimentally and analytically the bond between BFRP bars and GPC made from FA, GGBS and alkaline activator and cured at ambient temperature. Pull-out tests on ribbed BFRP bars with different bar diameters (6, 8, 10 mm) embedded in GPC cubes for different embedment lengths ($5d_b$, $10d_b$, $15d_b$) were conducted according to ACI 440.3R [41] to explore the bond behaviour in terms of average bond stress-slip curves at the bar free and loaded ends, bond strength, failure modes, and influences of bar diameter and embedment length. Afterwards, a bilinear model was proposed to theoretically describe the local bond-slip relationship of BFRP bars in GPC and closed-form solutions of the governing equations were developed to predict the interface properties. The bilinear model was validated against experimental data and then used to predict the tensile stress and bond stress distribution along the bar embedded portion. A parametric study was then carried out to estimate the influences of the involved bond-slip curve variables and the bar properties on the maximum pull-out load, based on which the underlying mechanisms of BFRP-GPC interaction were explored and discussed in depth.

2. Experimental program

2.1. Materials

2.2.1 Geopolymer concrete (GPC)

In this study, class F FA and GGBS, alkaline solution (AL), superplasticiser (SP), along with fine and coarse aggregates were used to prepare GPC. FA and GGBS were adopted as the precursors with a proportion of 85%:15% by mass. A combination of 10 molar sodium hydroxide (SH) solution and sodium silicate (SS) solution with a modulus (SiO_2/Na_2O) of 2.0 was used as the alkaline activator. The SH solution consisted of 31.40 wt% NaOH and 68.60 wt% H_2O, while the SS solution was composed of 30.71 wt% SiO_2, 15.36 wt% Na_2O and 53.93 wt% H_2O. The alkaline activator-to-binder (AL/B) ratio was 0.4. A modified polycarboxylate-based superplasticiser (SP) was added to improve the workability of GPC. Standard river sand with a nominal size of 0.03 - 2 mm was used as fine aggregates, while crushed limestone with a nominal maximum size of 20 mm was chosen as coarse aggregates (CA). Fine and coarse aggregates were used in saturated surface dry (SSD) condition according to ASTM C128 [42] and ASTM C127 [43], respectively. Table 1 shows the mix proportion of GPC adopted in this study, which was determined as reported in previous studies [44,45] considering the acceptable engineering properties in terms of workability, setting time and strengths.

Table 1. Mix proportion of geopolymer concrete.

FA (kg/m^3)	GGBS (kg/m^3)	SH (kg/m^3)	SS (kg/m^3)	SP (kg/m^3)	Sand (kg/m^3)	CA (kg/m^3)
340.00	60.00	53.00	107.00	4.00	632.50	1197.50

Note: FA (fly ash); GGBS (ground granulated blast-furnace slag); SH (sodium hydroxide); SS (sodium silicate); SP (superplasticizer); CA (coarse aggregate).

The mixing procedure for GPC is given as: (1) FA, GGBS, sand and coarse aggregates were mixed in the dry state for 3 min to ensure homogeneity of the mixture. Then, AL and SPs were added and mixed for another 3 min. (2) The moulds were coated with a thin oily film to facilitate the de-moulding procedure. (3) The fresh GPC was poured in two layers and vibrated for compaction. (4) The specimens were covered with a plastic film to avoid moisture loss and cured for 24 h at room temperature (20 ± 2 °C). (5) Afterwards, the specimens were de-moulded and cured in a standard curing room (20 ± 2 °C, 95% relative humidity) until the days of testing.

The workability of fresh GPC was determined with a slump test as per ASTM C143 [46]. The slump value of fresh GPC was 166 mm, indicating high workability according to the classification proposed by Talha Junaid et al. [47] for GPC. The hardened properties of GPC at 28 days including compressive strength, splitting tensile strength, and elastic modulus were measured in accordance with BS 12390 [48]. Three samples were tested for each property and the mean value was obtained and used. The compressive strength, splitting tensile strength, and elastic modulus of GPC were 42.34 MPa (±2.68 MPa), 3.57 MPa (±0.18 MPa), and 30.58 GPa (±0.76 GPa), respectively.

2.2.2 Basalt fibre reinforced polymer (BFRP) bar

Fig. 1 shows the ribbed BFRP bars used in this study, produced by pultrusion of continuous basalt fibres embedded in vinyl-ester. Three nominal diameters of 6, 8 and 10 mm were tested. The ribs with a smooth and round surface were obtained during pultrusion with a nylon laminate helically wrapped around the outside diameter. The rib depth was 6% of the diameter, which is considered to provide adequate bonding to concrete [49]. Five BFRP bars of 1000-mm length were prepared and tested according to ASTM D7205 [50] to determine effective diameter, tensile strength and elastic modulus. Due to their low transverse strength, an anchorage system was placed at the end of the bar between the bar and the tensile testing machine's jaws as a protection to prevent grip-induced damage, as recommended in ASTM D7205 [50]. Table 2 lists the results of the tested mechanical properties of BFRP bars under uniaxial tension.

As seen in Fig. 2, the BFRP bars exhibited a linear behaviour until failure and failed due to rupture of fibres. As expected, the tensile strength of the 10-mm bar (876 MPa) was 21% lower than that of the 8-mm bar (1117 MPa) due to potentially increased voids and defects with the increase of bar diameter [51,52]. However, unexpectedly, the tensile strength of the 6-mm bar was 899 MPa that is approximately 19% lower than that of the 8-mm bar. Fig. 2 also suggested a high variability in the stress-strain behaviour of different 6-mm bar samples at high stress levels. Such unexpected mechanical behaviour may be ascribed to the BFRP bars manufacturing method which could have led to some degree of inhomogeneous properties, as discussed in the following sections, and thus would affect the pull-out test results.

Fig. 1. Ribbed BFRP bars with various diameters.

Table 2. Physical and mechanical properties of BFRP bars.

Nominal diameter (mm)	Effective diameter (mm)	Ultimate tensile strength f_{fu} (MPa)	Elastic modulus E_b (GPa)
6	5.15	899.89	55.4
8	7.20	1117.58	58.2
10	8.00	876.37	57.5

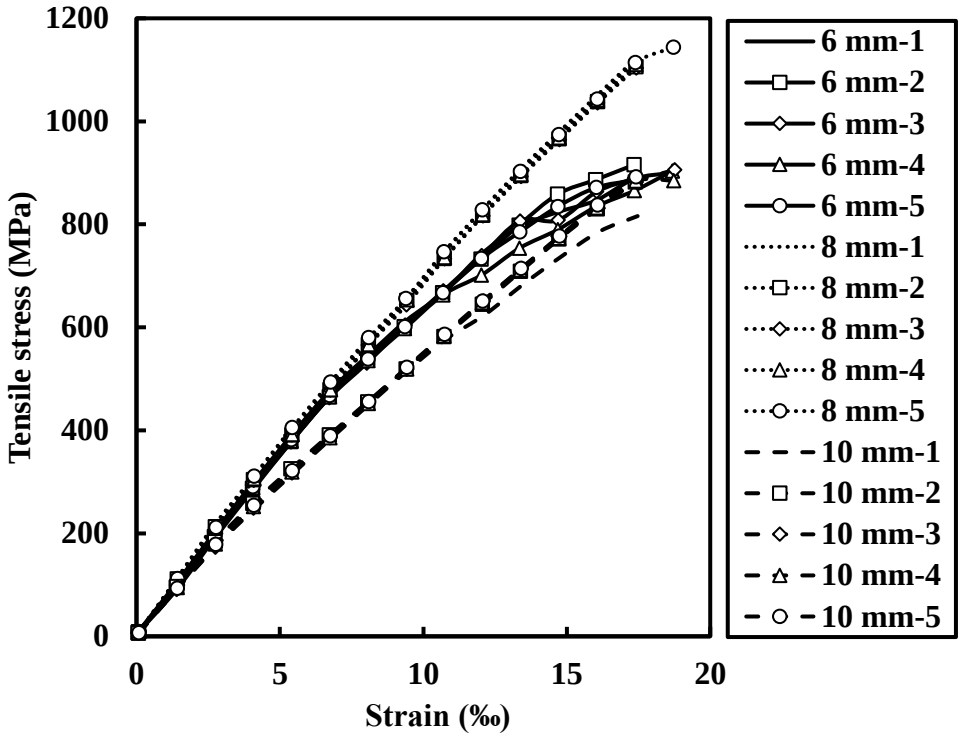

Fig. 2. Tensile behaviour of BFRP bars with various diameters.

2.2. Pull-out test

2.2.1 Sample preparation

The bond behaviour was investigated using pull-out tests on samples consisting of BFRP bars embedded at various depths in GPC cubes. The concrete was cast on a 150-mm cubic mould. A 700-mm long BFRP bar was placed horizontally, aligned transverse to the concrete casting direction. An anchorage was fitted at the bar loaded extremity to prevent damage, as discussed for the tensile test. Bond-breaker PVC tubes were fitted to the bar to obtain embedment lengths of $5d_b$, $10d_b$, $15d_b$. Three specimens were cast for each studied parameter to ensure data reliability. Each specimen was identified using a code that summarises the bar diameter, the embedment length, and the tested sample. For instance, the code 8-15d-1 represents a bar of 8-mm diameter and $15d_b$ embedment length, and the first sample tested.

2.2.2 Test method

Fig. 3 shows the pull-out test configuration. During testing, the samples were held by a frame made of two steel plates connected by four rods. The lower plate had a central hole to allow the bar to pass through. The upper plate had a pin on the top to be gripped by the testing machine upper jaw. The

relative slips between bar and concrete were recorded using linear variable displacement transducers (LVDT), one at the free end and three at the loaded end. A universal testing machine with a capacity of 1000 kN was arranged to apply the load to the bar under displacement control at 1.3 mm/min, as per ACI 440.3R [41]. At the end of pull-out tests, some samples were cut open to investigate the surface between concrete and bar, while other samples split open during the tests.

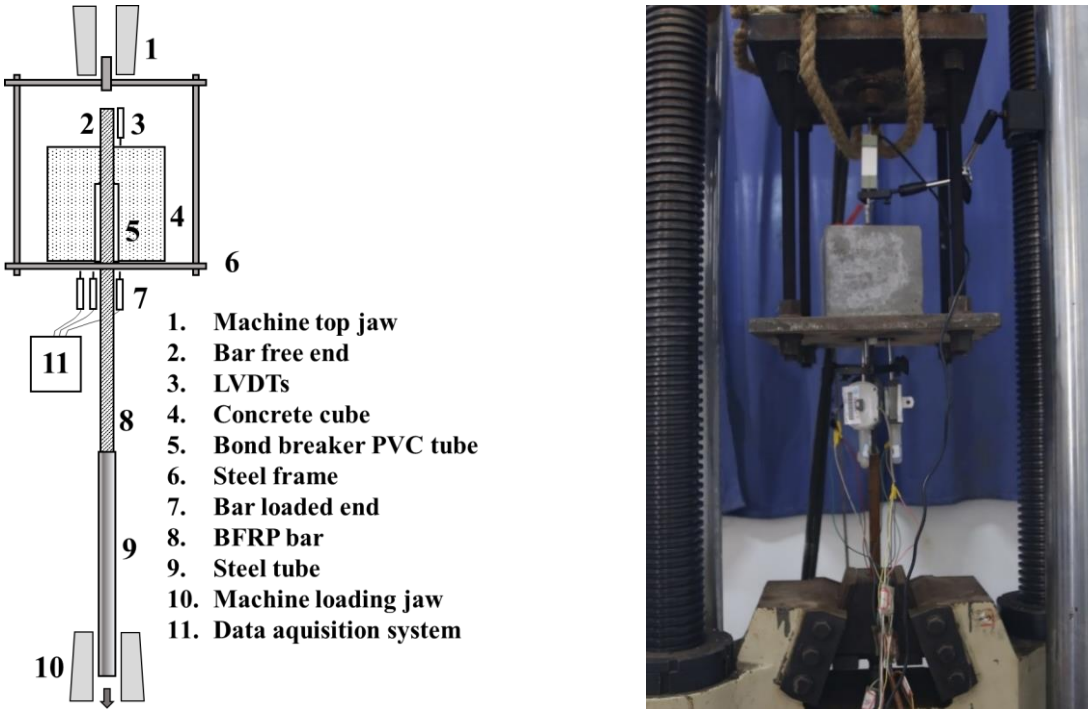

(a) (b)

Fig. 3. Pull-out test configuration: (a) graphical detail; (b) photo.

3. Experimental results and discussion

3.1. Bond stress-slip response

The experimental data of pull-out tests include tensile load applied and slips at the bar free end and loaded end. The average bond stress is defined as the shear force per area of bar-concrete interface, which can be calculated from the measured pull-out load as follows:

$$\tau = \frac{P}{\pi d_b l_d} \quad (1)$$

where τ is the average bond stress (MPa), P is the tensile load (N), d_b is the nominal bar diameter (mm) according to [21], and l_d is the embedded length (mm).

The average bond strength (τ_m) can be calculated by dividing the peak load (P_m) by the contact surface area. The results obtained from the pull-out tests are summarised in Table 3, including the failure mode (PO = pull-out of the bar, BF = failure of the bar, SC = splitting of concrete), the failure load (P_m), the average bond strength (τ_m), the coefficient of variation (COV) of the average bond strength, the slip at the free end ($s_{m,fe}$) for the maximum load, the slip at the loaded end ($s_{m,le}$) for

the maximum load, and the bond stress at the onset of slip at the loaded end ($\tau_{ons,le}$) and the free end ($\tau_{ons,fe}$).

Fig. 4 shows the average bond stress-slip curves of BFRP bars in GPC at both the free (FE) and loaded ends (LE) for various bar diameters and embedded lengths. As expected, there exist three typical stages. The chemical adhesion was lost immediately, as suggested by the low level of bond stress at the onset of the slip at the loaded end ($\tau_{ons,le}$), given in Table 3, ranging from 0.07 to 1.06 MPa. The early loss of chemical adhesion implies that the bond is mainly dependent on the mechanical interlock offered by the bar ribs and the concrete [53]. In the ascending branch, the stress increase was accompanied by a slip increase following a linear behaviour until the peak point. The linear ascending branch of BFRP bars in GPC is consistent with that observed for pull-out studies of similar materials such as GFRP bars in PCC [21,54].

After the peak point, the bond stress dropped sharply, followed by minor slippage for all the samples, except the sample 6-15d that exhibited a small region of constant stress level. The softening branches of the samples that failed due to bar rupture displayed a sharp reduction in the bond stress with limited slips, indicating the brittle failure along with a significant energy release. An obvious reduction in bond stress was also observed for the sample 8-5d which failed due to bar pull-out with a sudden loss of bond stress after the peak point. The sample 10-5d also failed due to bar pull-out but exhibited a more extended softening branch with a sharp falling slope. A similar bond loss along with small slips was illustrated during pull-out tests of BFRP bars in PCC cubes [25]. It is worth mentioning that the softening branch for the sample 10-15d was not recorded as the concrete cube split abruptly into two parts during the test.

Due to the low longitudinal elastic modulus of BFRP bars, there existed a difference between the slips measured at the bar ends, where the free end slipped at the maximum bond stress between 0.07 and 0.34 mm, and the loaded end slipped between 0.11 and 1.41 mm. Hence, the bond behaviour of BFRP bars was characterised by two curves, i.e. the bond stress-slip response at both the free and loaded ends. As soon as the pull-out test began, after the chemical adhesion between the bar and surrounding concrete was lost, the loaded end slip could be observed, and it increased rapidly. On the other hand, the onset of the slip at the free end happened at a higher level of stress, as seen in Fig. 4, and it developed at a slower pace than that at the loaded end. The difference between the slips at free and loaded ends implies the nonlinear distribution of shear bond stress along the BFRP bar embedded portion, which can be attributed to the peak bond stress moving progressively towards the bar free end as the load increases [55].

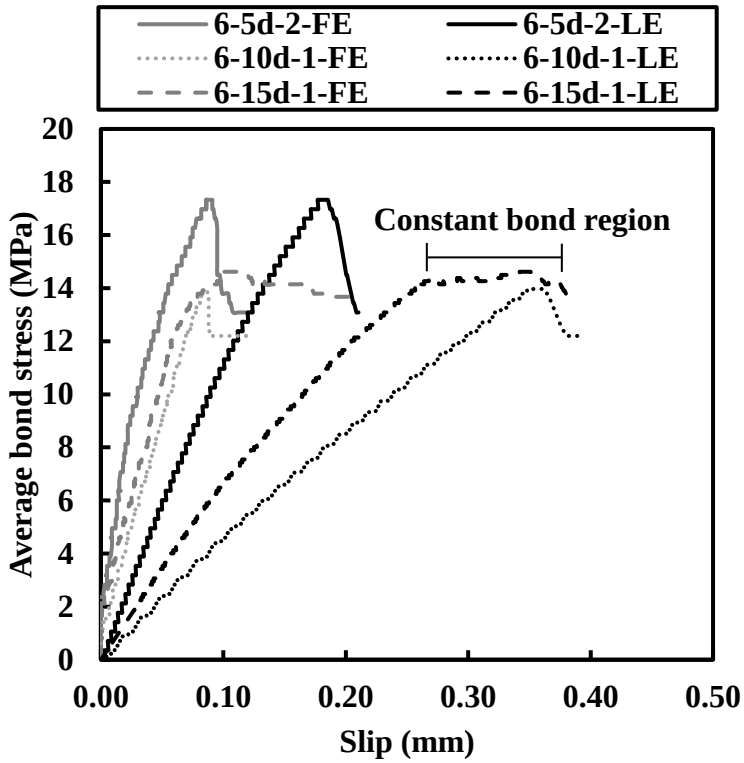
6-5d-2-FE
6-5d-2-LE
6-10d-1-FE
6-10d-1-LE
6-15d-1-FE
6-15d-1-LE
Constant bond region
Average bond stress (MPa)
Slip (mm)
0
2
4
6
8
10
12
14
16
18
20
0.00
0.10
0.20
0.30
0.40
0.50

(a)

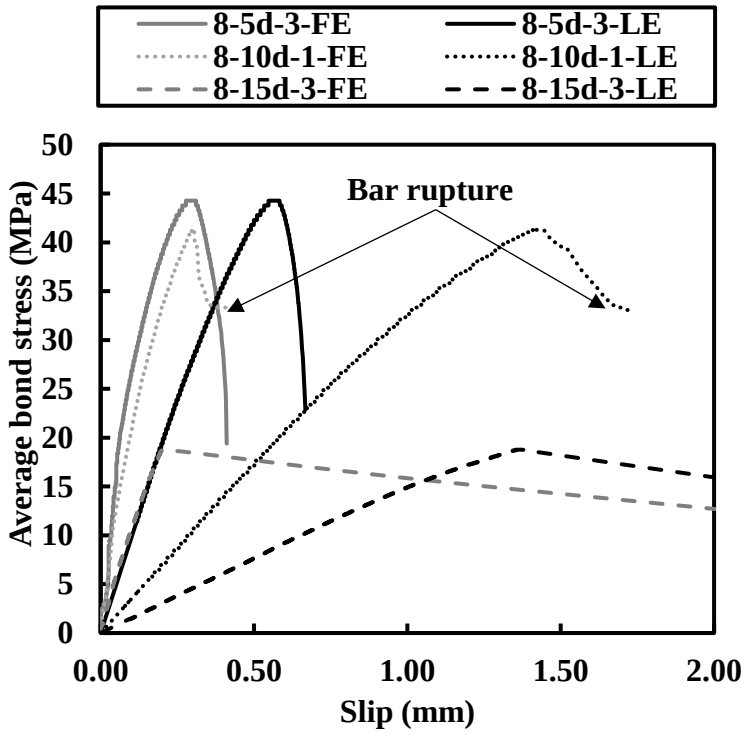
8-5d-3-FE
8-5d-3-LE
8-10d-1-FE
8-10d-1-LE
8-15d-3-FE
8-15d-3-LE
Bar rupture
Average bond stress (MPa)
Slip (mm)
0
5
10
15
20
25
30
35
40
45
50
0.00
0.50
1.00
1.50
2.00

(b)

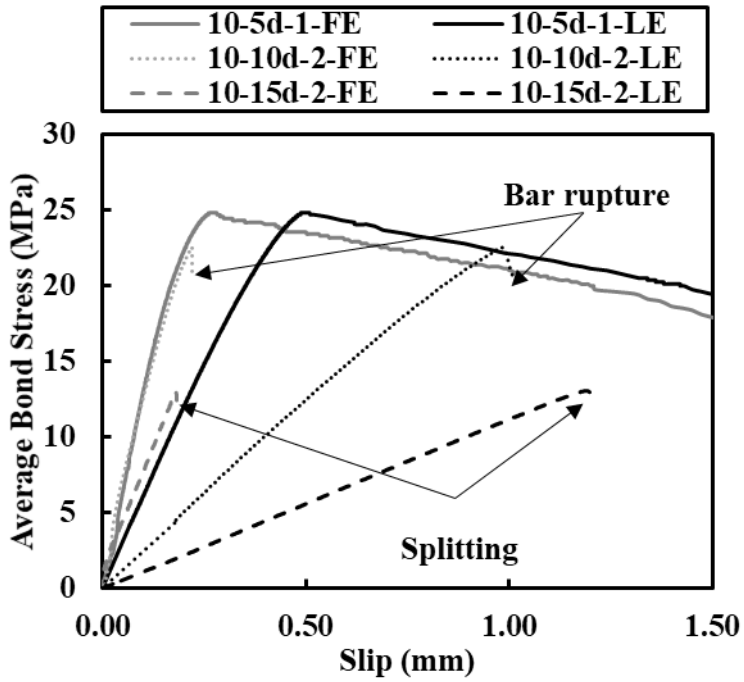

(c)

Fig. 4. Average bond stress-slip curves at the free end (FE) and the loaded end (LE) of BFRP bar samples with different embedment lengths and diameters of (a) 6 mm; (b) 8 mm; (c) 10 mm.

Table 3. Pull-out test results.

Sample	Failure	P_m (kN)	τ_m (MPa)	COV	$s_{m,le}$ (mm)	$s_{m,fe}$ (mm)	$\tau_{ons,le}$ (MPa)	$\tau_{ons,fe}$ (MPa)
6-5d-1	PO/BF	8.20	14.50		0.13	0.07	0.71	2.12
6-5d-2	PO/BF	9.80	17.33	12.3%	0.18	0.09	0.35	3.18
6-5d-3	PO/BF	7.80	13.79		0.11	0.08	1.06	2.83
6-10d-1	PO/BF	15.60	13.79		0.34	0.08	0.18	1.59
6-10d-2	PO/BF	18.40	16.27	16.5%	0.40	0.08	0.18	2.30
6-10d-3	PO/BF	13.20	11.67		0.30	0.08	0.35	0.71
6-15d-1	PO/BF	24.80	14.62		0.34	0.11	0.35	2.59
6-15d-2	PO/BF	24.20	14.26	1.2%	0.38	0.11	0.35	0.71
6-15d-3	PO/BF	24.60	14.50		0.38	0.21	0.35	3.18
8-5d-1	PO	41.50	41.28		0.57	0.33	0.50	1.49
8-5d-2	PO	41.00	40.78	4.5%	0.59	0.34	0.50	1.49
8-5d-3	PO	44.50	44.26		0.55	0.28	0.50	2.49
8-10d-1	BF	83.00	41.28		1.41	0.30	0.25	1.49
8-10d-2	BF	82.00	40.78	0.9%	1.34	0.28	0.25	1.49
8-10d-3	BF	83.50	41.53		1.36	0.24	0.25	6.71
8-15d-1	PO	57.00	18.90		1.25	0.13	0.17	1.16
8-15d-2	PO	56.60	18.77	0.4%	1.35	0.20	0.07	0.93
8-15d-3	PO	56.60	18.77		1.35	0.20	0.13	0.86
10-5d-1	PO	39.00	24.83		0.49	0.26	0.38	0.51
10-5d-2	PO	44.60	28.39	8.6%	0.60	0.34	0.38	2.55
10-5d-3	PO	38.20	24.32		0.54	0.30	0.25	1.02
10-10d-1	BF	72.80	23.17		1.14	0.30	0.13	0.25
10-10d-2	BF	70.80	22.54	3.7%	0.98	0.22	0.13	0.19
10-10d-3	BF	67.60	21.52		1.04	0.24	0.13	0.38
10-15d-1	SC	50.40	10.70		0.95	0.14	0.08	0.64
10-15d-2	SC	61.40	13.03	11.6%	1.18	0.18	0.08	1.15
10-15d-3	SC	62.60	13.28		1.21	0.19	0.17	0.93

3.2. Bond strength

Table 4 summarises the sample repetitions, the total number of tests and the COV of the present study in comparison with those of available studies of pull-out tests on steel and FRP bars embedded in concrete blocks [17,56–58]. The COV of average bond strength was found to be between 0.4% and 16.5%, suggesting good repeatability of the failure load for BFRP bars in GPC and good agreement with that reported in the reference studies. The effects of different factors on bond strength of BFRP bars in GPC are analysed and discussed in detail below.

Table 4. Comparison of COV of maximum bond stress with existing studies.

Ref.	Material	Concrete	Sets	Repetitions	Total number of tests	COV
Present work	B, S	GPC	14	3	27	0-17%
El Refai et al. (2015)	B, G	PCC	16	3	48	2-30%
Baena (2010)	C, G, S	PCC	23	2 or 3	88	1-41%
Tekle et al. (2016)	G	GPC	9	3	27	4-16%
Ahmed et al. (2008)	C, G, S	PCC	8	5	40	2-21%

Note: B = basalt FRP, G = glass FRP, C = carbon FRP, S = steel, PCC = Portland cement concrete, GPC = geopolymer concrete.

3.2.1. Effect of embedment length

Fig. 5a shows the effect of BFRP bar embedment length in GPC on bond strength, which indicates that the increase of bar embedment length from $5d_b$ to $15d_b$ resulted in a reduction of the average bond strength of 52% for 8-mm bars and 55% for 10-mm bars, respectively, while only 5% reduction of bond strength can be observed for 6-mm bars. The reduction in bond strength with the increase of embedment length can be attributed to the nonlinear distribution of bond stress along the bar-concrete interface and a more extensive surface area of contact between bar and concrete which lowers the average bond strength. The changing trend observed for BFRP bars in GPC agrees with the findings of pull-out studies on similar materials such as BFRP bars in PCC [17] where an average bond strength reduction of up to 29% was reported, and different FRP bars in PCC [53,55]. The embedded length also influences the mode of failure, as discussed in Section 3.3.

3.2.2. Effect of bar diameter

Fig. 5b shows the effect of BFRP bar diameter on bond strength, indicating a reduction of bond strength with increasing diameter, which is consistent with the findings on BFRP bars in PCC [59], CFRP bars in PCC [53], and GFRP bars in GPC [57]. The bond strength for 10-mm bars were about 34% to 46% lower than that for 8-mm bars with the same embedded length. The bond strength drop with increasing diameter can be ascribed to the nonlinear distribution of stress along the concrete-bar interface, the shear lag effect and the Poisson's effect. Nevertheless, the 6-mm bars unexpectedly exhibited an average bond strength of about 23% to 66% lower than 8-mm bars, which can be attributed to the premature failure caused by bar rupture. As discussed in Section 2.1, the 6-mm bars have relatively lower mechanical properties, which could lead to a detrimental effect on their bond performance. For clarity reasons, the data of the 6-mm samples were not included in Fig. 5b.

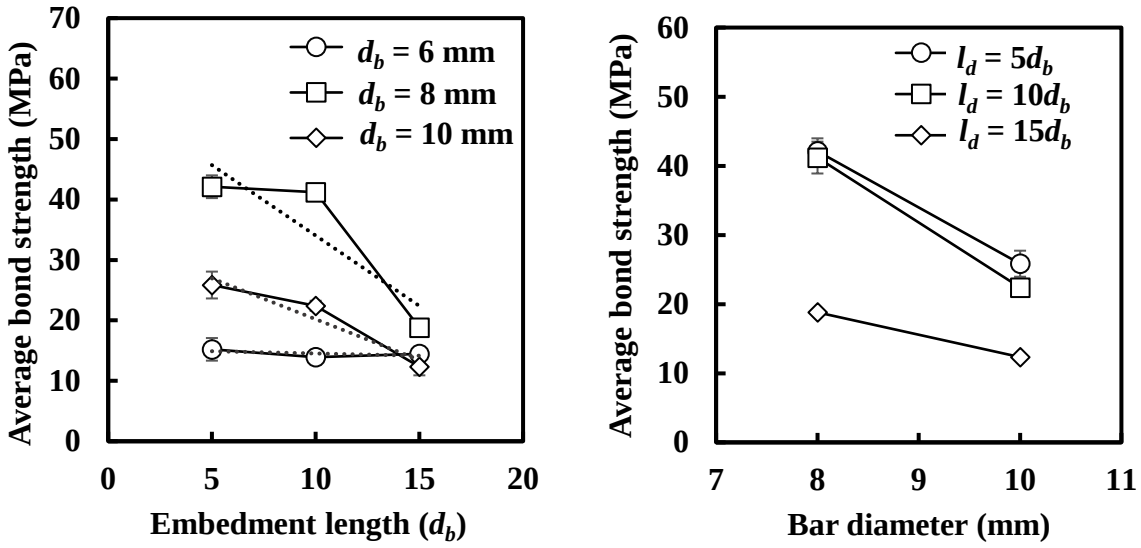

(a) (b)

Fig. 5. Average bond strength between BFRP bar and geopolymer concrete against: (a) embedment length; (b) bar diameter.

3.3. Failure modes

Fig. 6 shows the typical failure modes of the BFRP bar pull-out tests, including bar pull-out, concrete splitting, and bar rupture. The failure mode was affected by the embedment length. Shorter embedment length ($5d_b$), e.g. in samples 8-5d and 10-5d, provided insufficient interaction area between BFRP bars and GPC, leading to pull-out failure. Bar pull-out is experienced when the embedded length is shorter than the development length [38], representing the minimum length of the bar embedded in the concrete capable of developing the strength necessary to transfer the tensile force from the reinforcement to the concrete.

Fig. 6a shows the sample 8-5d cut open to inspect the interface zone between the bar and the concrete, indicating that the pull-out failure was due to concrete lugs shearing off, causing the embedded concrete surface to become smooth, while the bar ribs were intact, implying a high shear strength good integrity between the ribs and the successive bar layers. The pull-out failure usually occurs at the interface when the shear bond strength between the bar and surrounding concrete is exceeded. When the concrete provides an adequate amount of confinement to prevent splitting, the cracks remain limited to the portion surrounding the bar, leading to a pull-out failure [16]. Bar pull-out is the preferred type of failure during pull-out tests, as it provides an estimation of the bonding between bar and concrete. On the other hand, concrete splitting and bar rupture are considered premature failures as the interface between bar and concrete is still intact after the sample failure.

Fig. 6b shows the sample 10-15d that splitted open during the test, suggesting that the longer embedment length ($15d_b$) would cause concrete splitting. Only a thin layer of concrete can be found on the bar surface while the bar surface and the concrete at the interface were still intact, indicating

that the maximum bond strength was not attained. The splitting failure is associated with the poor confinement. The radial stress originated by the tensile pull-out load generates some cracks at the interface between the rebar and the surrounding concrete. When the concrete confinement is not sufficient to bear the radial stress and the concrete tensile strength is reached, the cracks propagate towards the concrete surface, resulting in splitting failure while the interface zone with the reinforcement remains intact. The present findings are consistent with the behaviour observed for GFRP bars in PCC [38,60] and GFRP bars in GPC [61,62].

Fig. 6c and d display the failure of specimens induced by bar rapture, which occurs when the bond is adequate, and the pull-out load reaches the bar tensile strength leading to its failure in tension. Some samples (6-15 and 10-10) failed due to bar rupture at the expected tensile stress, while others underperformed or exceeded the tensile strength. For instance, the samples 6-5d and 6-10d failed respectively at a load of 66% and 38% lower than the expected one, while the samples 8-10 overperformed and failed at a load level 46% higher than the expected one. Overall, all 6-mm BFRP bars failed due to bar rupture, regardless of the embedment length. The variability of bond performance can be ascribed to the variations of tensile stress-strain behaviour for 6-mm bars discussed in Section 2.1.

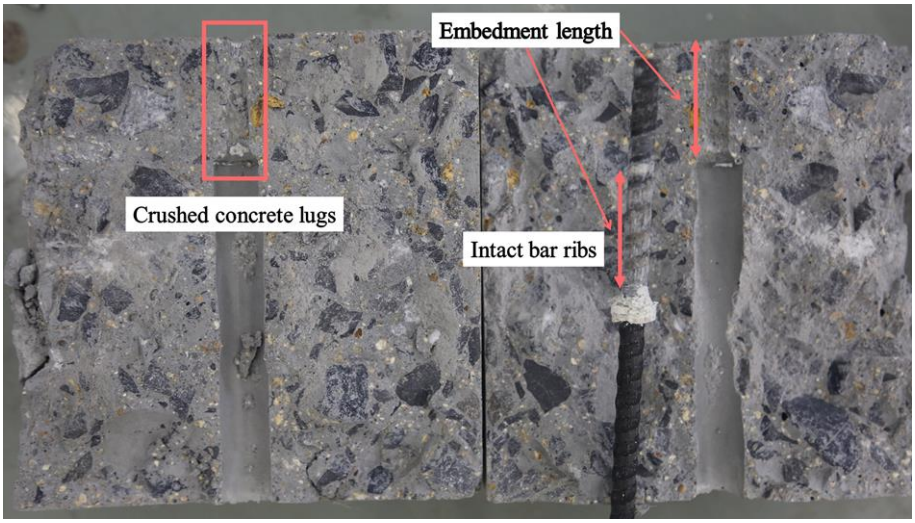

(a)

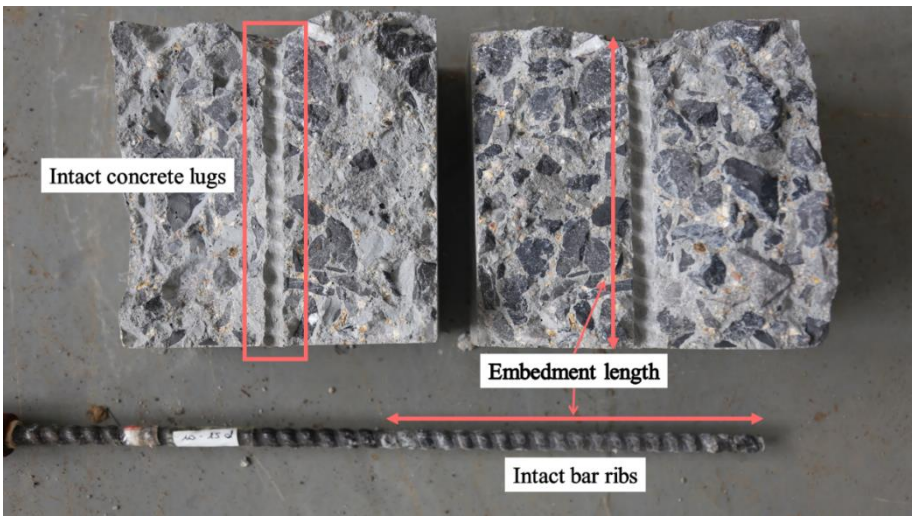

(b)

(c)

Fig. 6. Typical failure modes under pull-out tests due to: (a) pull-out of the bar for sample 8-5d; (b) splitting of concrete for sample 10-15d; (c) bar rupture in tension for samples 6-5d and 8-10d.

4. Theoretical analysis of bond behaviour of BFRP bars in GPC

As introduced above, the available analytical models for the bond-slip response of FRP bars in concrete, i.e. mBPE and CMR models, present a nonlinear behaviour in the ascending branch [20,34]. However, as the experimental data of BFRP bars in GPC suggested a linear behaviour both in the ascending and descending phases, a bilinear model in calibration with experimental results is proposed here to describe the bond stress-slip relationship, which can also be used for finite element modelling of the pull-out test of BFRP bars in GPC. Furthermore, closed-form solutions are developed, allowing to predict the stress and strain distribution along the bar embedded length in GPC.

4.1. Bilinear local bond stress-slip model

Fig. 7 illustrates the bilinear model proposed to describe the bond stress-slip relationship for BFRP bars in GPC. The bond-slip curve can be expressed as:

$$\tau(s) = \begin{cases} ks & 0 \le s \le s_m \\ \dfrac{\tau_m}{s_d}(s_m + s_d - s) & s_m \le s \le s_u \end{cases} \quad (2)$$

where τ is the bond stress (MPa), $k = \tau_m/s_m$ is the bond stiffness (N/mm^3), τ_m is the maximum bond stress (MPa), s is the slip of the bar (mm), s_m is the slip at the maximum bond stress that is generally determined at the free end of the bar [20], and $s_d = s_u - s_m$ where s_u is the ultimate slip (mm).

Fig. 8 shows a schematic illustration of a bar embedded in concrete during the pull-out process under a tensile load. The bond stress acting on the contact surface between bar and concrete is $\tau = \tau(s)$, where the slip $s = s(x)$ represents the relative displacement between bar and concrete at a location x and $\sigma = \sigma(x)$ denotes the tensile stress at the location x, being x a reference axis along the bar. The equilibrium of a small length dx of a bar with diameter d_b in terms of the tensile stress acting on the bar cross-sectional area and the shear stress acting on the contact surface between the bar and the concrete can be described as [63]:

$$\tau(s_b(x))\pi d_b dx = \frac{\pi d_b^2}{4} d\sigma(x) \tag{3}$$

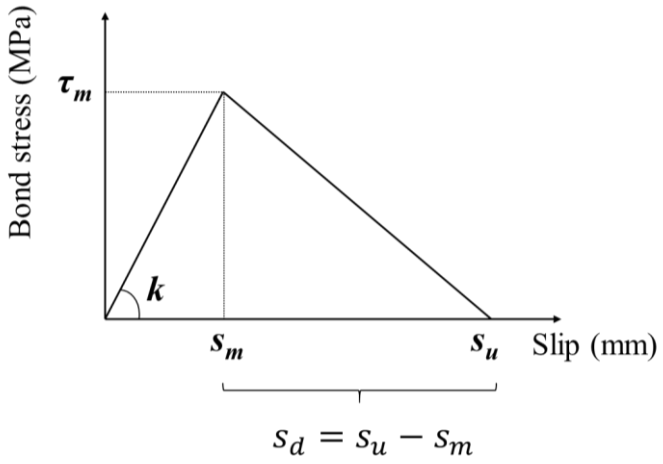

Fig. 7. Bilinear bond stress-slip relationship.

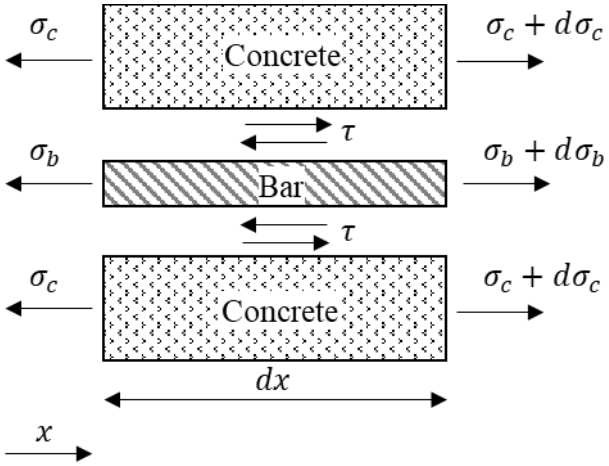

Fig. 8. Equilibrium of bar element embedded in concrete under uniaxial tensile force.

As per previous studies [39,64], two assumptions are made herein: the BFRP bar along the longitudinal direction is considered to be linear elastic, and the deformation of concrete is ignored as

the displacement of concrete at the interface between bar and concrete can be negligible if compared to the displacements of the points of the bar.

The slip, strain, bond stress and tensile stress for the ascending branch can be expressed as:

$$s(x) = c_1 \cosh(\lambda_1 x) + c_2 \sinh(\lambda_1 x) \quad (4)$$

$$\frac{ds(x)}{dx} = \lambda_1 c_1 \sinh(\lambda_1 x) + \lambda_1 c_2 \cosh(\lambda_1 x) \quad (5)$$

$$\tau(x) = k[c_1 \cosh(\lambda_1 x) + c_2 \sinh(\lambda_1 x)] \quad (6)$$

$$\sigma(x) = E_b[\lambda_1 c_1 \sinh(\lambda_1 x) + \lambda_1 c_2 \cosh(\lambda_1 x)] \quad (7)$$

where $\lambda_1 = \sqrt{\frac{4\,k}{E_b d_b}}$, E_b is the bar elastic modulus (MPa), and d_b is the bar diameter (mm).

For the descending branch, the bond properties can be given as:

$$s(x) = c_3 \sin(\lambda_2 x) + c_4 \cos(\lambda_2 x) + s_m + s_d \quad (8)$$

$$\frac{ds(x)}{dx} = \lambda_2 c_3 \cos(\lambda_2 x) - \lambda_2 c_4 \sin(\lambda_2 x) \quad (9)$$

$$\tau(x) = -\frac{\tau_m}{s_d}[c_3 \sin(\lambda_2 x) + c_4 \cos(\lambda_2 x)] \quad (10)$$

$$\sigma(x) = E_b[\lambda_2 c_3 \cos(\lambda_2 x) - \lambda_2 c_4 \sin(\lambda_2 x)] \quad (11)$$

where $\lambda_2 = \sqrt{\frac{\tau_m}{s_d}\frac{4}{E_b d_b}}$.

The constants c_1, c_2, c_3 and $c_4$can be determined considering the boundary conditions at the bar free end ($x = 0$) and loaded end ($x = l_d$) listed below:

$$\left.\frac{ds_b}{dx}\right|_{x=0} = \varepsilon_b(0) = 0 \quad (12)$$

$$\left.\frac{ds_b}{dx}\right|_{x=l_d} = \varepsilon_b(l_d) = \frac{P}{E_b A_b} \quad (13)$$

4.2. Comparison of theoretical predictions with experimental data

The proposed model was applied to the experimental results of the pull-out of BFRP bars in GPC, and the validity of the theoretical predictions was assessed. For comparison purposes, the sample 10-5d-1 was chosen within those that failed due to bar pull-out, providing a close estimation of the bond strength, the results of which are shown in Fig. 9. It can be seen that the proposed model offered the predictions of bond-slip curve with satisfactory accuracy in terms of values and shape compared to the experimental data. The predictions scored a root-mean-square error of 5% for the bond-slip curve at the free end and 8% for that at the loaded end. After such validation, the theoretical formulation was then used to predict the distribution of bond stress and tensile stress along the bar embedded portion, which is presented below.

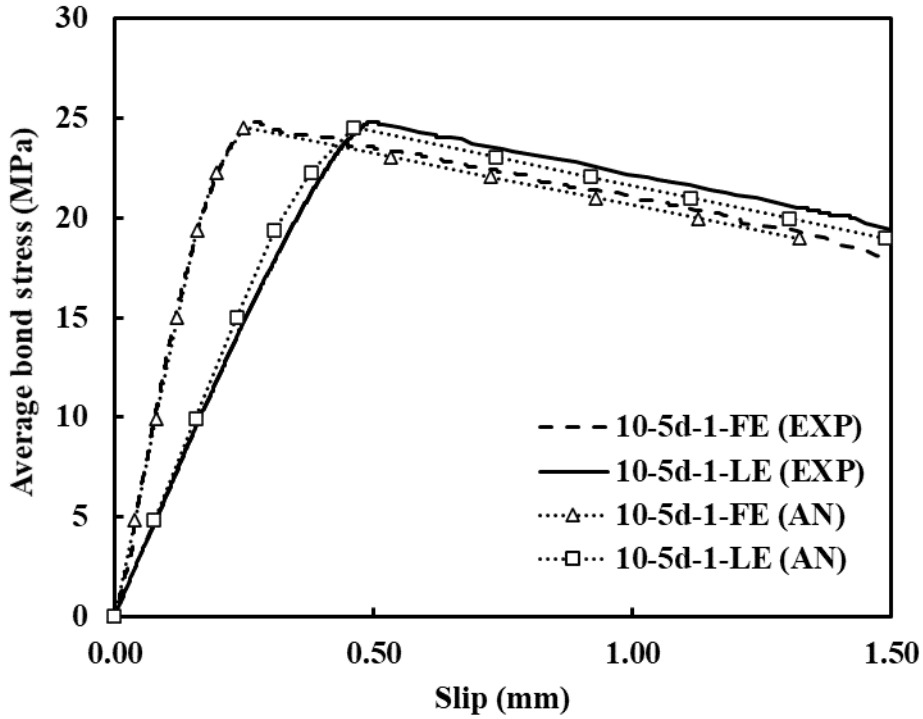

Fig. 9. Comparison between experimental and analytical bond-slip response for sample 10-5d-1.

4.3. Bond interface properties

Fig. 10a displays the bar normal tensile stress, which increased with the load level and decreased from the loaded end towards the free end. The tensile stress tended to be nonlinear for lower pull-out loads but constant for higher pull-out loads. As shown in Fig. 10b, the bond stress along the bar increased with increasing pull-out load until the maximum bond stress was reached. For lower pull-out loads (20% - 60% P_m), the peak bond stress was found at the bar loaded end, and by increasing the load level, the peak bond stress reached the maximum bond stress and progressively migrated towards the bar free end, suggesting a nonlinearity of the bond behaviour along the bar embedment length. It is worth noting that the bond stress distribution along longer embedment lengths can vary compared to the average bond stress. Thus, following the recommendations by [35–37], the shorter embedment length (~$5d_b$) was considered to obtain a relatively uniform bond stress distribution, as indicated in Fig. 10b for the case of 10-5d, which was found to be similar to the experimental value (24.83 MPa) provided in Table 3.

Fig. 11 shows the bond stress concentration factor (K_c), i.e. the ratio of the predicted peak bond stress to the average bond stress, at different load levels. A parametric study was run to estimate the variation of K_c for different bar diameters (8 and 10 mm) and embedment lengths ($5d_b$, $10d_b$, $15d_b$) whilst maintaining the bond-slip parameters. K_c increased with increasing bar diameter and embedment length and reduced with increasing load. At low load levels (20% P_m), a high K_c was

found, with values ranging from 1.50 to 3.93, and it approached 1.0 with the increase of pull-out load. This trend indicated a strong nonlinearity of the bond stress profile at lower load levels and a more even distribution for higher loads, consistent with that illustrated in Fig. 10b. Furthermore, the changes of K_c with bar diameter and embedment length can be observed at lower loading stages, while for higher load levels (80% - 100% P_m) all samples displayed a similar K_c.

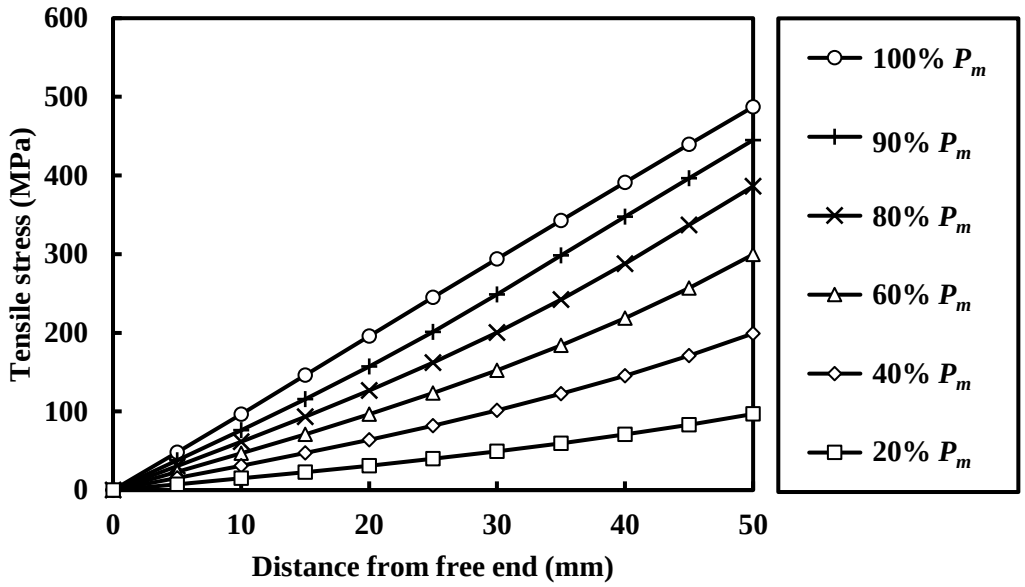

(a)

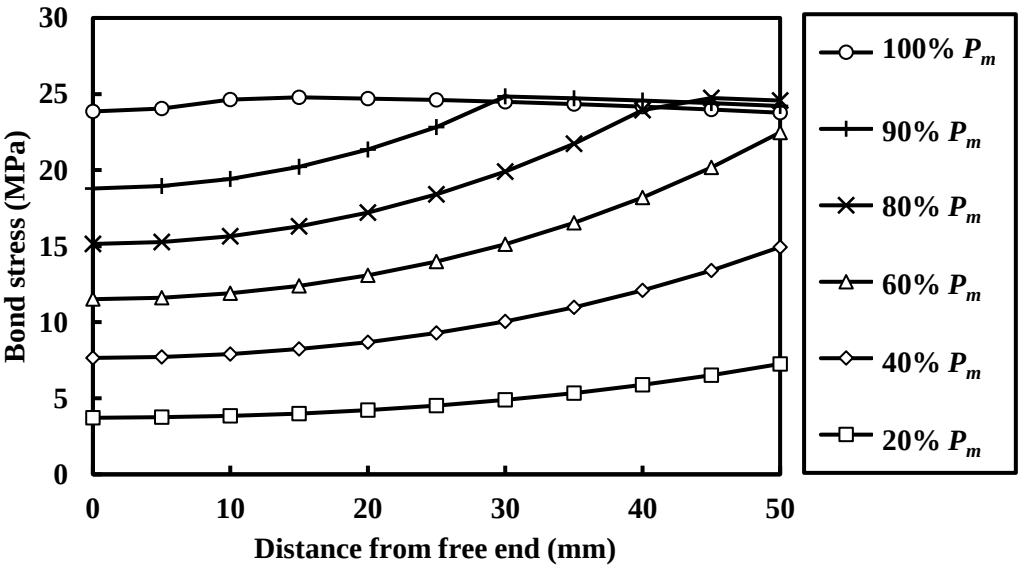

(b)

Fig. 10. Theoretical predictions of stress distribution for sample 10-5d-1: (a) tensile stress; (b) bond stress.

To investigate the radial bond stress profile along the bar embedment length at different loading levels, finite element modelling of pull-out process of BFRP bars in GPC for the sample 10-5d was performed, the results of which are shown in Fig. 12. In fact, the bond force develops at an angle α

to the bar axis, which can therefore be divided into two components, the shear bond stress (τ) as discussed above, and the radial bond stress (σ_r), being the latter normal component. The radial bond stress generated by the wedging actions of the bar ribs acts as a splitting pressure on the concrete and is resisted by the tensile hoop stress [65]. The angle α depends on the surface profile of BFRP bar, and higher values of α suggest an increasing tendency to splitting. A smooth bar is expected to develop no radial stress (α = 0°) while for sand coated GFRP bars, α = 30° can be adopted, and for ribbed bars, the values of α up to 60° can be used [66]. Being the two stress components related to each other as $\sigma_r = \tau \tan(\alpha)$, an average angle α = 42° was estimated for the sample 10-5d, indicating a good mechanical interlocking offered by the surface ribs of BFRP bars, as discussed in Section 3.1.

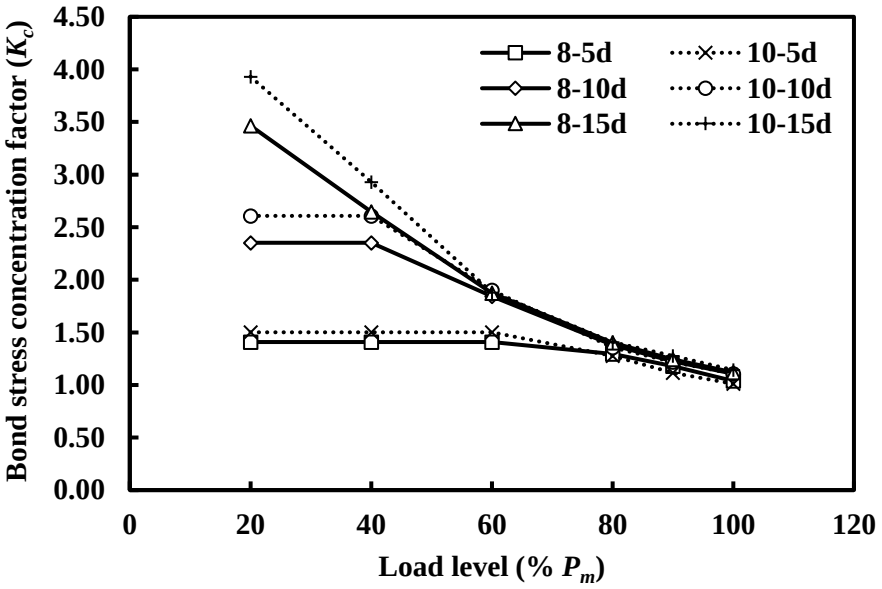

Fig. 11. Variation of bond stress concentration factor with load level for different bar diameters and embedment lengths.

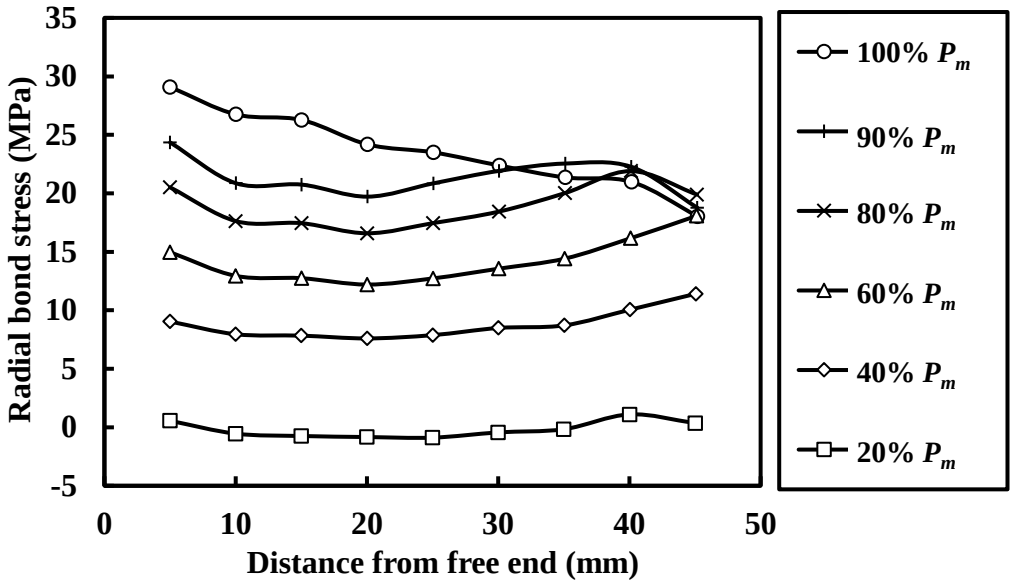

Fig. 12. Numerical predictions of radial bond stress distribution for sample 10-5d-1.

4.4. Parametric study on maximum pull-out load

After the validations of bond-slip model, a parametric study was carried out to estimate the influences of different parameters considered in the theoretical equations on the maximum pull-out load, including the parameters characterising the bond-slip curve, namely, slip at peak, ultimate slip and bond strength, as well as the diameter, embedment length, and elastic modulus of BFRP bar. For parametric study, the value of each parameter varied while the other parameters remained unchanged.

4.4.1. Effect of bond-slip curve parameters

First, the sensitivity of the theoretical predictions to the input parameters for bond-slip curve was evaluated and shown in Fig. 13. As seen in Fig. 13a, the value of the slip at peak (s_m) varied between 0.1 and 0.5 mm, and the value of the ultimate slip (s_u) changed from 5 to 9 mm, which have been chosen based on the study on pull-out of BFRP bars in PCC [17]. The bond strength (τ_m) was in the range of 20 and 30 MPa. As indicated in Fig. 13a and b, the slip at peak and the ultimate slip had no significant influence on the maximum pull-out load. Nevertheless, the maximum pull-out load was increased linearly with the increase of bond strength (see Fig. 13c), suggesting that the theoretical predictions are sensitive to the input bond-slip curve, which should be calibrated on the specific experimental conditions, limiting the theoretical predictions.

4.4.2. Effects of bar diameter and embedment length

Different bar diameters ranging from 6 to 20 mm with an increment of 2 mm, and embedment lengths in the range of 5 - $20d_b$ with an increment of $2.5d_b$ were adopted to estimate the effects of bar diameter and embedment length on maximum pull-out load, which are the most commonly used ranges to investigate the bond between BFRP bars and concrete [17,18,59,67]. The results shown in Fig. 13d and e indicate that both the bar diameter and embedment length have a significant influence on the maximum pull-out load that rised obviously with the increase of bar diameter and embedment length. The predicted bond strength reduced less significantly compared to the experimental data: it was reduced by about 5% with the increase of bar diameter from 6 to 10 mm and by about 11% as the embedment length increases from $5d_b$ to $15d_b$. The lower reduction in bond strength with increasing bar diameter and embedment length obtained from theoretical predictions than experimental data can be attributed to the sensitivity of theoretical predictions to the bond-slip parameters, as discussed above.

4.4.3. Effect of bar elastic modulus

Fig. 13f shows the variation of maximum pull-out load with the elastic modulus of BFRP bar ranging from 30 to 80 GPa, which are commonly reported in the literature on BFRP bars [17,68–73]. For BFRP bars in GPC, the predicted maximum pull-out load remained relatively constant, regardless of the bar elastic modulus, implying that the elastic modulus of BFRP bar has no significant influence on the maximum pull-out load. A similar conclusion was drawn in literature for materials comparable

to those investigated here that the changes in elastic moduli of GFRP bars from 30 to 65 GPa [35] and 42 to 50 GPa [61] have a negligible influence on the maximum pull-out load of GFRP bars in concrete and GPC, respectively.

However, BFRP bars have a lower elastic modulus than conventional steel rebars [16]. Fig. 14 shows a comparison of the bond stress distribution of the 10-mm BFRP bar with an elastic modulus of 57.5 GPa for the sample 10-5d-1 with that of steel rebar which has an elastic modulus of 210 GPa but the same configurations. The distribution of bond stress along the bar embedded in GPC was remarkably influenced by its elastic modulus, where the stiffer steel rebar provided a more constant bond stress distribution along the embedded length in comparison with the more uneven distribution exhibited by the BFRP bar with a relatively lower elastic modulus. Therefore, the nonlinearity of the bond stress between BFRP bars and GPC can be attributed to the bar elastic modulus, similarly to the findings for GFRP bars in PCC [40].

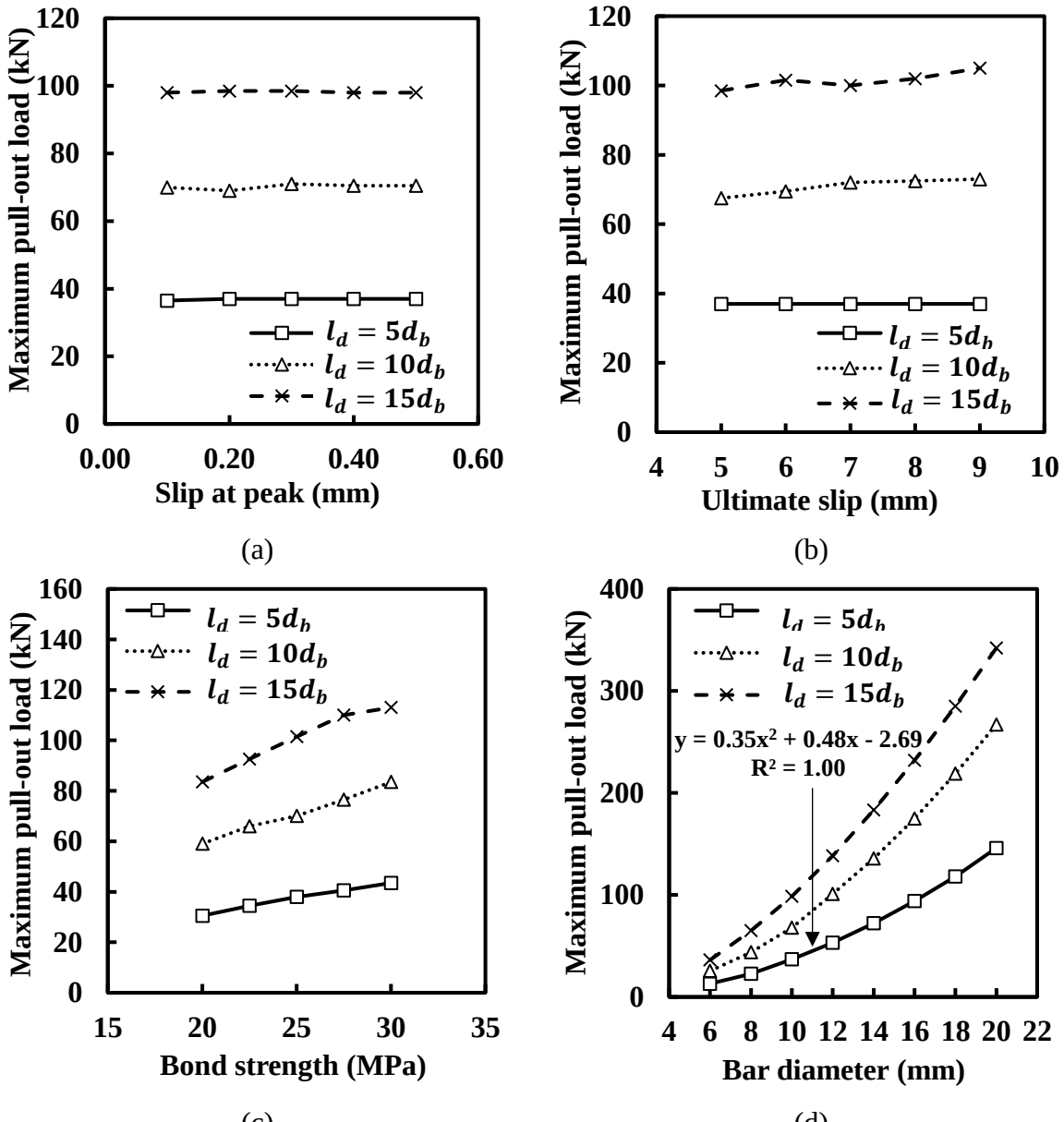

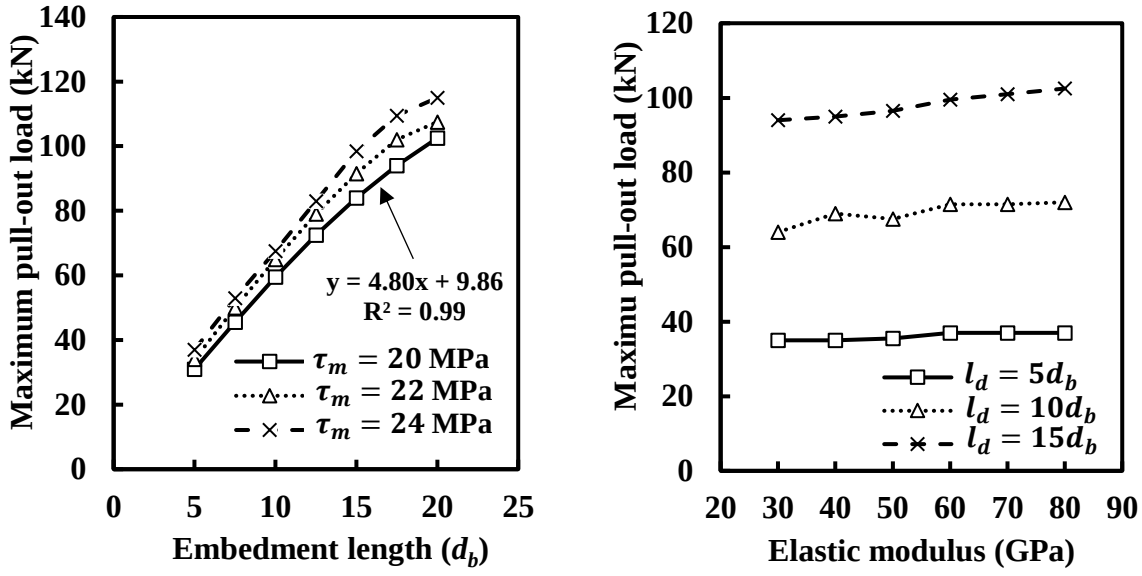

(e) (f)

Fig. 13. Variation of pull-out load with: (a) slip at peak; (b) ultimate slip; (c) bond strength; (d) bar diameter; (e) embedment length; (f) bar elastic modulus.

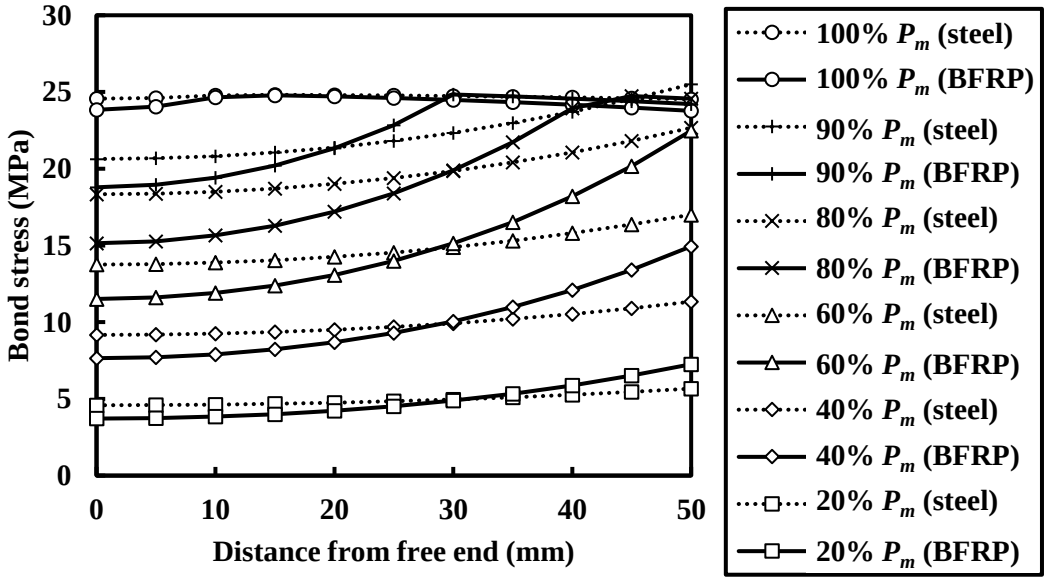

Fig. 14. Comparison between bond stress distribution of BFRP bar and steel bar for sample 10-5d-1.

4.5. Theoretical predictions of bond strength

According to the above paramedic study, only the bar diameter and embedment length among the parameters evaluated exhibited a significant influence on the maximum pull-out load. Therefore, the bond strength of BFRP bars in GPC was expressed as a function of bar diameter (d_b) and embedment length (l_d) by fitting the obtained data shown in Fig. 13 as follows:

$$\tau = -0.0162d_b^2 + 0.41793d_b - 0.42526l_d + 23.2037 \quad (14)$$

In Table 5, the experimental bond strengths of BFRP bars in GPC are compared with the predictions obtained from available standard codes for FRP bars as internal reinforcement as well as

that by Eq. (14). The relevant recommendations of ACI 440 [74], CSA S806-02 [75], CSA S6-14 [76], and JSCE [77] for predictions are given in Eqs. (15)-(18), respectively:

$$\frac{\tau}{0.083\sqrt{f_c}} = 4.0 + 0.3\frac{c}{d_b} + 100\frac{d_b}{l_d} \quad (15)$$

$$\tau = \frac{d_{cs}\sqrt{f_c}}{1.15\,k_1k_2k_3k_4k_5\,\pi\,d_b} \quad (16)$$

$$\tau = \frac{f_{cr}d_{cs}}{0.45\pi d_b k_1k_6k_7} \quad (17)$$

$$\tau = f_{bod}/\alpha_1 \quad (18)$$

where τ is the average bond stress developed (MPa), c is the concrete cover dimension (mm), f_c is the concrete compressive strength (MPa), k_1 is the bar location factor equal to 1.0, k_2 is the concrete density factor equal to 1.0, k_3 is the bar size factor equal to 0.8, k_4 is the bar fibre factor assumed equal to 1.0, k_5 is the bar surface profile equal to 1.05, d_{cs} is the smallest of the distance from the closest concrete surface to the centre of the bar being developed which shall not be taken greater than $2.5d_b$, k_6 is the coating factor equal to 1.0, k_7 is the bar size factor equal to 0.8, f_{cr} is the tensile strength of the concrete and equal to $0.4\sqrt{f_c}$ where the value of $\sqrt{f_c}$ shall not exceed 8.0 MPa. For the JSCE code, α_1 is the modification factor equal to 0.6, f_{bod} is the design bond strength of concrete (MPa) calculated as $f_{bod} = \alpha_2\left(0.28\frac{f_{ck}^{2/3}}{\gamma_c}\right)$ where the value of f_{bod} shall not exceed 3.2 MPa, α_2 is the modification factor equal to 1.0, f_{ck} is the characteristic value for concrete compressive strength (MPa), and γ_c is the safety coefficient for concrete equal to 1.3. Regarding the CSA S6 and JSCE codes, they consider the confining effect offered by the transverse reinforcement which was neglected in this study since no stirrups were used in the tested samples.

As indicated in Table 5, the CSA S806, CSA S6 and JSCE codes provided similar values of predicted bond strength, regardless of the variations of bar diameter and embedded length, which is due to the limitations imposed on the concrete cover c for the Canadian standards (CSA S806 and CSA S6) and α_1 for the Japanese standard (JSCE). Furthermore, the influence of embedment length on bond strength is neglected in both CSA S806 and JSCE. On the contrary, the prediction by ACI 440 considered the effect of the embedment length and thus, a reduction in predicted bond strength with the increase of embedment length can be observed. However, as per the other design codes, no difference was found between different bar diameters as the effect of bar diameter was not considered due to the limitation imposed to the ratio c/d_b. All design codes provided conservative estimations of the bond strength between BFRP bars and GPC, where CSA S806, CSA S6 and JSCE seem to be too conservative and CSA S6 is the most conservative one. ACI 440.1R offered still conservative but more accurate predictions of bond strength.

The predictions of bond strength using Eq. (14) show a closer estimation to experimental data, with an average ratio of experimental to predicted bond strength of 1.07 against those ranging from 2.62 to 5.46 obtained using the standard provisions. Nonetheless, some of the predicted values seem to be non-conservative, especially those for the 6-mm bar samples which failed prematurely due to bar rupture, and that for the sample 10-15d with a failure of concrete splitting. Therefore, Eq. (14) can be considered a preliminary equation for predicting the bond strength of BFRP bars in GPC, which can be further modified to consider more experimental data for calibration.

Table 5. Comparison of experimental bond strength with predictions from standard codes and regression analysis equation.

	EXP	ACI 440.1R		CSA S806		CSA S6		JSCE		Eq. (14)	
Sample	τ_{exp}	τ_{pred}	τ_{exp}/τ_{pred}	τ_{pred}	τ_{exp}/τ_{pred}	τ_{pred}	τ_{exp}/τ_{pred}	τ_{pred}	τ_{exp}/τ_{pred}	τ_{pred}	τ_{exp}/τ_{pred}
6-5d	15.21	13.15	1.16	5.21	2.92	5.59	2.72	4.20	3.62	23.00	0.66
6-10d	13.91	7.90	1.76	5.21	2.67	5.59	2.49	4.20	3.31	20.88	0.67
6-15d	14.46	6.15	2.35	5.21	2.78	5.59	2.59	4.20	3.44	18.75	0.77
8-5d	42.11	13.15	3.20	5.21	8.08	5.59	7.53	4.20	10.03	23.38	1.80
8-10d	41.20	7.90	5.21	5.21	7.91	5.59	7.37	4.20	9.81	21.26	1.94
8-15d	18.81	6.15	3.06	5.21	3.61	5.59	3.36	4.20	4.48	19.13	0.98
10-5d	25.85	13.15	1.97	5.21	4.96	5.59	4.62	4.20	6.16	23.64	1.09
10-10d	22.41	7.90	2.84	5.21	4.30	5.59	4.01	4.20	5.34	21.51	1.04
10-15d	12.34	6.15	2.01	5.21	2.37	5.59	2.21	4.20	2.94	19.38	0.64
AVERAGE			2.62		4.40		4.10		5.46		1.07
SD			1.18		2.20		2.05		2.73		0.49
COV			45%		50%		50%		50%		46%

5. Conclusions

In this paper, a series of pull-out tests were carried out to investigate the bond behaviour of BFRP bars in GPC, considering the effects of bar diameter (d_b) and embedment length (l_d). Afterwards, a bilinear bond-slip model was proposed to describe the bond-slip behaviour of BFRP bars in GPC. According to the experimental results and the theoretical analysis, the main conclusions can be drawn as follows:

- The bond of BFRP bars in GPC occurs mainly by the mechanical interlocking of the bar ribs instead of chemical adhesion as indicated in the low bond stress at loaded end slip onset. The bond-slip curve consists of a linear ascending branch followed by a sudden loss in bond stress along with small slippage for all the samples, except the sample 6-15d exhibiting a small region of constant stress level. The bilinear model proposed to describe the bond-slip curve analytically shows a good agreement with experimental data with a root-mean-square error of about 5% for the curve at the free end and 8% for the curve at the loaded end.

- The bar diameter and embedment length have a significant influence on the bond behaviour in terms of average bond strength and failure patterns. As the bar diameter increases from 8 to 10 mm, the average bond strength is reduced by 34-46%. Increasing the bar embedment length from $5d_b$ to $15d_b$ results in a reduction of the average bond strength by 5%, 52% and 55% for the 6-mm, 8-mm and 10-mm bars, respectively. The failure modes include bar pull-out, concrete splitting, and bar rupture. Shorter embedment length ($5d_b$) leads to pull-out failure due to insufficient contact area between BFRP bars and GPC, while longer embedment length ($15d_b$) causes concrete splitting. The pull-out failure can be ascribed to the crushing of the concrete lugs while no damage can be found on the reinforcement surface, suggesting high shear strength of the BFRP bar ribs. All samples containing 6-mm BFRP bars fail due to bar rupture, regardless of the embedment length.
- There exists a non-linear distribution of bond stress along the embedded BFRP bars in GPC as indicated in the difference in slips at the bar free and loaded ends. According to the theoretical predictions, the bond stress concentration factor that represents the ratio of the bond strength to the average bond stress at a specific load level at low load levels varies from 1.50 to 3.93, suggesting a high nonlinearity of the bond stress profile, which can be attributed to the low elastic modulus of BFRP bars as demonstrated in the parametric study.
- An empirical equation was proposed to predict the bond strength of BFRP bars in GPC considering the effects of bar diameter and embedment length. The predictions of bond strength using this equation agree well with experimental data as compared with the estimations by the available recommendations for FRP bars in concrete which are too conservative.

Acknowledgements

The authors gratefully acknowledge the financial support from the Engineering and Physical Sciences Research Council (EPSRC) under Grant Nos. EP/R041504/1 and 1836739 as well as the Royal Society under Award No. IEC\NSFC\191417. The financial support provided by the British Council and China Scholarship Council (CSC) to the first author is also gratefully acknowledged.

References

[1] Barcelo L, Kline J, Walenta G, Gartner E. Cement and carbon emissions. Mater Struct 2014;47:1055–65. https://doi.org/10.1617/s11527-013-0114-5.

[2] Shi C, Jiménez AF, Palomo A. New cements for the 21st century: The pursuit of an alternative to Portland cement. Cem Concr Res 2011;41:750–63. https://doi.org/10.1016/j.cemconres.2011.03.016.

[3] Davidovits J. Geopolymer cement to minimize carbon-dioxde greenhouse-warming. Ceram Trans · 1993;37:165–82.

[4] Broomfield JP. Corrosion of steel in concrete: Understanding, investigation and repair. London:

1997.

[5] Bowman E, Jacobson G, Koch G, Varney J, Thopson N, Moghissi O, et al. NACE International IMPACT International Measures of Prevention, Application, and Economics of Corrosion Technologies Study. 2016.

[6] Serbescu A, Guadagnini M, Pilakoutas K. Mechanical characterization of basalt FRP rebars and long-term strength predictive model. J Compos Constr 2014;19. https://doi.org/10.1061/(ASCE)CC.1943-5614.

[7] Fan X, Zhang M. Experimental study on flexural behaviour of inorganic polymer concrete beams reinforced with basalt rebar. Compos Part B Eng 2016;93:174–83. https://doi.org/10.1016/j.compositesb.2016.03.021.

[8] Fan X, Zhang M. Behaviour of inorganic polymer concrete columns reinforced with basalt FRP bars under eccentric compression: An experimental study. Compos Part B Eng 2016;104:44–56. https://doi.org/10.1016/j.compositesb.2016.08.020.

[9] Fan X, Zhou Z, Tu W, Zhang M. Shear behaviour of inorganic polymer concrete beams reinforced with basalt FRP bars and stirrups. Compos Struct 2021;255:112901. https://doi.org/10.1016/j.compstruct.2020.112901.

[10] Sturm AB, Visintin P. Local bond slip behavior of steel reinforcing bars embedded in ultra high performance fibre reinforced concrete. Struct Concr 2019;20:108–22. https://doi.org/10.1002/suco.201700149.

[11] Fernández-Jiménez A, Palomo A. Engineering properties of alkali-activated fly. ACI Mater J 2006;103:106–12.

[12] Shi C, Xie P. Interface between cement paste and quartz sand in alkali-activated slag mortars. Cem Concr Res 1998;28:887–96. https://doi.org/10.5833/jjgs.31.591.

[13] Lee WKW, Van Deventer JSJ. The interface between natural siliceous aggregates and geopolymers 2004;34:195–206. https://doi.org/10.1016/S0008-8846(03)00250-3.

[14] Castel A, Foster SJ. Bond strength between blended slag and Class F fly ash geopolymer concrete with steel reinforcement. Cem Concr Res 2015;72:48–53. https://doi.org/10.1016/j.cemconres.2015.02.016.

[15] CEB-FIP. Bulletin 40 - FRP reinforcement for RC structures. Fib Bull 2007:160.

[16] CEB-FIP. Bulletin 10 - Bond of reinforcement in concrete. Fib Bull 2000;10:427.

[17] El Refai A, Ammar M-A, Masmoudi R. Bond performance of basalt fiber-reinforced polymer bars to concrete. J Compos Constr 2015;19. https://doi.org/10.1061/(ASCE)CC.1943-5614.0000487.

[18] Wang L, Song Z, Yi J, Li J, Fu F, Qian K. Experimental Studies on Bond Performance of BFRP Bars Reinforced Coral Aggregate Concrete. Int J Concr Struct Mater 2019;13:52.

https://doi.org/10.1186/s40069-019-0367-7.

[19] Wang H, Sun X, Peng G, Luo Y, Ying Q. Experimental study on bond behaviour between BFRP bar and engineered cementitious composite. Constr Build Mater 2015;95:448–56. https://doi.org/10.1016/j.conbuildmat.2015.07.135.

[20] Cosenza E, Manfredi G, Realfonzo R. Behavior and modeling of bond of FRP rebars to concrete. J Compos Constr 1997;1:40–51. https://doi.org/10.1061/(ASCE)1090-0268(1997)1:2(40).

[21] Baena M, Torres L, Turon A, Barris C. Experimental study of bond behaviour between concrete and FRP bars using a pull-out test. Compos Part B 2009;40:784–97. https://doi.org/10.1016/j.compositesb.2009.07.003.

[22] Dong Z, Wu G, Lian J. Experimental study on the durability of FRP bars reinforced concrete beams in simulated ocean environment. IEEE J Sel Top Quantum Electron 2018;25:1123–34. https://doi.org/10.1515/secm-2017-0237.

[23] Altalmas A, El Refai A, Abed F. Bond degradation of basalt fiber-reinforced polymer (BFRP) bars exposed to accelerated aging conditions. Constr Build Mater 2015;81:162–71. https://doi.org/10.1016/j.conbuildmat.2015.02.036.

[24] Hassan M, Benmokrane B, ElSafty A, Fam A. Bond durability of basalt-fiber-reinforced-polymer (BFRP) bars embedded in concrete in aggressive environments. Compos Part B Eng 2016;106:262–72. https://doi.org/10.1016/j.compositesb.2016.09.039.

[25] El Refai A, Abed F, Altalmas A. Bond durability of basalt fiber–reinforced polymer bars embedded in concrete under direct pullout conditions. J Compos Constr 2015;19:04014078. https://doi.org/10.1061/(asce)cc.1943-5614.0000544.

[26] Marchand P, Baby F, Khadour A, Battesti T, Rivillon P, Quiertant M, et al. Bond behaviour of reinforcing bars in UHPFRC. Mater Struct 2016;49:1979–95. https://doi.org/10.1617/s11527-015-0628-0.

[27] Rolland A, Quiertant M, Khadour A, Chataigner S, Benzarti K, Argoul P. Experimental investigations on the bond behavior between concrete and FRP reinforcing bars. Constr Build Mater 2018;173:136–48. https://doi.org/10.1016/j.conbuildmat.2018.03.169.

[28] Malek A, Scott A, Pampanin S, Hoult NA. Postyield Bond Deterioration and Damage Assessment of RC Beams Using Distributed Fiber-Optic Strain Sensing System. J Struct Eng 2019;145:1–17. https://doi.org/10.1061/(ASCE)ST.1943-541X.0002286.

[29] Lee B, Mulheron M. Fluctuation of bond stress-slip behaviour of deformed bar under displacement control. Mag Concr Res 2012;64:863–75. https://doi.org/10.1680/macr.9.00209.

[30] Henault J, Quiertant M, Delepine-lesoille S, Salin J, Moreau G, Taillade F, et al. Quantitative strain measurement and crack detection in RC structures using a truly distributed fiber optic sensing system. Constr Build Mater 2012;37:916–23.

https://doi.org/10.1016/j.conbuildmat.2012.05.029.

[31] Lee B, Mulheron M. Measurement of bar strain during pull-out tests: Use of electrical resistance gauge methods under large displacement. Mag Concr Res 2015;67:523–31. https://doi.org/10.1680/macr.13.00201.

[32] Malvar LJ. Bond stress-slip characteristics of FRP rebars. TR-2013-SHR Nav Facil Eng Serv Center, Port Hueneme, CA 1994.

[33] Eligehausen R, Popov EP, Bertero V V. Local bond stress-slip relationships of deformed bars under generalized excitations: Experimental results and analytical model. UCB/EERC-83/23, Univ California, Earthq Eng Res Centre, Berkeley, CA 1983:1983.

[34] Cosenza E, Manfredi G, Realfonzo R. Analytical modelling of bond between FRP reinforcing bars and concrete. Non-Metalic Reinf Concr Struct Reinf Concr Struct 1995:164–71. https://doi.org/10.1145/2505515.2507827.

[35] Mazaheripour H, Barros JAO, Sena-Cruz J, Soltanzadeh F. Analytical Bond Model for GFRP Bars to Steel Fiber Reinforced Self-Compacting Concrete. J Compos Constr 2013;17. https://doi.org/10.1061/(asce)cc.1943-5614.0000399.

[36] Lu ZH, Wu SY, Tang Z, Zhao YG, Li W. Effect of chloride-induced corrosion on the bond behaviors between steel strands and concrete. Mater Struct Constr 2021;54:1–16. https://doi.org/10.1617/s11527-021-01724-8.

[37] Ling Y, Wang K, Li W, Shi G, Lu P. Effect of slag on the mechanical properties and bond strength of fly ash-based engineered geopolymer composites. Compos Part B Eng 2019;164:747–57. https://doi.org/10.1016/j.compositesb.2019.01.092.

[38] Pecce M, Manfredi G, Realfonzo R, Cosenza E. Experimental and analytical evaluation of bond properties of GFRP bars. J Mater Civ Eng 2001:282–90.

[39] Focacci F, Nanni A, Bakis CE. Local bond-slip relationship for FRP reinforcement in concrete. J Compos Constr 2000:24–31.

[40] Fava G, Carvelli V, Pisani MA. Remarks on bond of GFRP rebars and concrete. Compos Part B Eng 2016;93:210–20. https://doi.org/10.1016/j.compositesb.2016.03.012.

[41] ACI. ACI 440.3R-04 - Guide test methods for fiber-reinforced polymers (FRPs) for reinforcing or strengthening concrete structures. 2004.

[42] ASTM C128. Standard Test Method for Relative Density (Specific Gravity) and Absorption of Fine Aggregate. ASTM Int 2015. https://doi.org/10.1520/C0128-15.2.

[43] ASTM C127. Standard Test Method for Relative Density (Specific Gravity) and Absorption of Coarse Aggregate. ASTM Int 2015. https://doi.org/10.1520/C0127-15.2.

[44] Fang G, Ho WK, Tu W, Zhang M. Workability and mechanical properties of alkali-activated fly ash-slag concrete cured at ambient temperature. Constr Build Mater 2018;172:476–87.

https://doi.org/10.1016/j.conbuildmat.2018.04.008.

[45] Zhong H, Zhang M. Effect of recycled tyre polymer fibre on engineering properties of sustainable strain hardening geopolymer composites. Cem Concr Compos 2021;122: 104167. https://doi.org/10.1016/j.cemconcomp.2021.104167.

[46] ASTM C143/C143M-15. Standard Test Method for Slump of Hydraulic-Cement Concrete 2015. https://doi.org/10.1520/C0143.

[47] Talha Junaid M, Kayali O, Khennane A, Black J. A mix design procedure for low calcium alkali activated fly ash-based concretes. Constr Build Mater 2015;79:301–10. https://doi.org/10.1016/j.conbuildmat.2015.01.048.

[48] British Standards Institution BSI. BS EN 12390 - Testing hardened concrete. 2012.

[49] Achillides Z. Bond behaviour of FRP bars in concrete. PhD Thesis, Fac Eng Univ Sheffield, UK 1998.

[50] ASTM D7205. Standard test methods for tensile properties of fiber reinforced polymer matrix composite bars, American Society for Testing and Materials, Conshohocken, USA. ASTM Int 2011.

[51] Adhikari S. Mechanical properties and flexural applications of basalt fiber reinforced polymer (BFRP) bars. 2009.

[52] Bank LC. Composites for Construction: Structural Design with FRP Materials. 2006. https://doi.org/10.1002/9780470121429.

[53] Achillides Z, Pilakoutas K. Bond Behavior of Fiber Reinforced Polymer Bars under Direct Pullout Conditions. J Compos Constr 2004;8:173–81. https://doi.org/10.1061/(asce)1090-0268(2004)8:2(173).

[54] Rezazadeh M, Carvelli V, Veljkovic A. Modelling bond of GFRP rebar and concrete. Constr Build Mater 2017;153:102–16. https://doi.org/10.1016/j.conbuildmat.2017.07.092.

[55] Benmokrane B, Tighiouart B, Chaallal O. Bond Strength and Load Distribution of Composite GFRP Reinforcing Bars in Concrete. ACI Mater J 1996;93:254–9. https://doi.org/10.14359/9810.

[56] Baena M. Study of bond behaviour between FRP reinforcement and concrete. PhD Thesis, Univ Girona 2010.

[57] Tekle BH, Khennane A, Kayali O. Bond properties of sand-coated GFRP bars with fly ash-based geopolymer concrete. J Compos Constr 2016;20(5). https://doi.org/10.1061/(ASCE)CC.

[58] Ahmed EA, El-Salakawy EF, Benmokrane B. Bond Stress-Slip Relationship and Development Length of FRP Bars Embedded in Concrete. HBRC J 2008;4.

[59] Li C, Gao D, Wang Y, Tang J. Effect of high temperature on the bond performance between basalt fibre reinforced polymer (BFRP) bars and concrete. Constr Build Mater 2017;141:44–51.

https://doi.org/10.1016/j.conbuildmat.2017.02.125.

[60] Yan F, Lin Z, Yang M. Bond mechanism and bond strength of GFRP bars to concrete: A review. Compos Part B Eng 2016;98:56–69. https://doi.org/10.1016/j.compositesb.2016.04.068.

[61] Tekle BH. Bond behaviour of GFRP bars embedded in alkali activated cement concrete. 2017. https://doi.org/10.1016/j.conbuildmat.2017.08.029.

[62] Maranan GB, Manalo AC, Karunasena W, Benmokrane B. Pullout behaviour of GFRP bars with anchor head in geopolymer concrete. Compos Struct 2015;132:1113–21. https://doi.org/10.1016/j.compstruct.2015.07.021.

[63] Russo G, Zingone G, Romano F. Analytical solution for bond-slip of reinforcing bars in R. C. joints. J Struct Eng 1990;116:336–55.

[64] Yuan H, Teng JG, Seracino R, Wu ZS, Yao J. Full-range behavior of FRP-to-concrete bonded joints 2004;26:553–65. https://doi.org/10.1016/j.engstruct.2003.11.006.

[65] Tepfers T. Cracking of concrete cover along anchored deformed reinforcing bars. Mag Concr Res 1979;31.

[66] Tepfers R, Karlsson M. Pull-out and tensile reinforcement splice tests using FRP C-Bars. Third Int. Symp. Non-Metallic Reinf. Concr. Struct., 1997, p. 357–64.

[67] Yang S, Yang C, Huang M, Liu Y, Jiang J, Fan G. Study on bond performance between FRP bars and seawater coral aggregate concrete. Constr Build Mater 2018;173:272–88. https://doi.org/10.1016/j.conbuildmat.2018.04.015.

[68] Elgabbas F, Ahmed EA, Benmokrane B. Physical and mechanical characteristics of new basalt-FRP bars for reinforcing concrete structures. Constr Build Mater 2015;95:623–35. https://doi.org/10.1016/j.conbuildmat.2015.07.036.

[69] Ali AH, Mohamed HM, Benmokrane B, ElSafty A, Chaallal O. Durability performance and long-term prediction models of sand-coated basalt FRP bars. Compos Part B Eng 2019;157:248–58. https://doi.org/10.1016/j.compositesb.2018.08.065.

[70] Fan X, Xu T, Zhou Z, Zhou X. Experimental Study on Basic Mechanical Properties of BFRP Bars. IOP Conf Ser Mater Sci Eng 2017;250. https://doi.org/10.1088/1757-899X/250/1/012014.

[71] Patnaik A, Banibayat P, Adhikari S, Robinson P. Mechanical Properties of Basalt Fiber Reinforced Polymer Bars Manufactured Using a Wet Layup Method. Int Rev Civ Eng 2012;3:412–7.

[72] Alnajmi L, Abed F. Evaluation of FRP bars under compression and their performance in RC columns. Materials (Basel) 2020;13:1–19. https://doi.org/10.3390/ma13204541.

[73] Liu X, Wang X, Xie K, Wu Z, Li F. Bond Behavior of Basalt Fiber-Reinforced Polymer Bars Embedded in Concrete Under Mono-tensile and Cyclic Loads. Int J Concr Struct Mater 2020;14. https://doi.org/10.1186/s40069-020-0394-4.

[74] ACI 440.1R. Guide for the design and construction of structural concrete reinforced with FRP bars. Am Concr Inst 2015:88. https://doi.org/10.1061/40753(171)158.

[75] CAN/CSA S806-02. Design and construction of building structures with fibre-reinforced polymers. Can Stand Assoc 2002.

[76] CAN/CSA-S6-14. Canadian Highway Bridge Design Code. Can Stand Assoc 2017;Reprinted.

[77] JSCE. Recommendations for design and construction of concrete structures using continuous fiber reinforcing materials. Concrete Engineering Series, 23, Tokyo, Japan: Research Committee on Continuous Fiber Reinforcing Materials; 1997. Japanese Soc Civ Eng 1997.